SUPPLEMENTARY MATERIAL

The third KV62 radar scan: Searching for hidden chambers adjacent to Tutankhamun's tomb.

1. Data acquisition

The wooden frame was designed for HF scans is reported in Figure 1S.

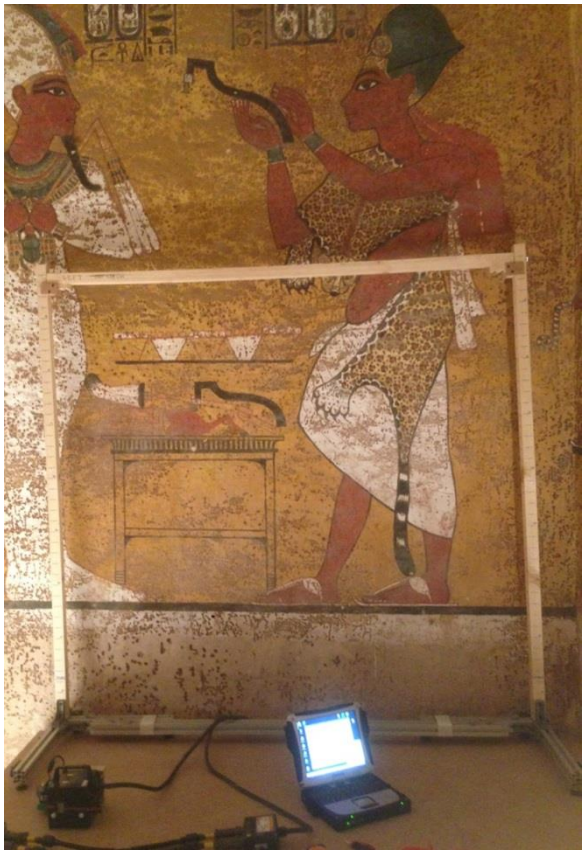

Figure 1S: *Picture taken during HF radar scans showing the wood frame over the wooden platform in the right side of the North wall where the sealed doorways is supposed.*

This frame was used starting from the third day of the surveys in an attempt to attenuate the significant diffractions from the vertical lateral supports observed in the radargrams during the first two days, which were performed with a similar aluminum frame. Given the presence the sarcophagus lid resting on the floor

of the burial chamber, we also built a wooden platform to pass over it (Figure 1S). In order to compensate for the highly irregular floor surface, we leveled a wooden slab that we used as base for the frame.

The GPR profiles distribution for the LF dataset is shown in Figure 2S, where the white arrows represent the position of the radargrams collected along the KV62 walls.

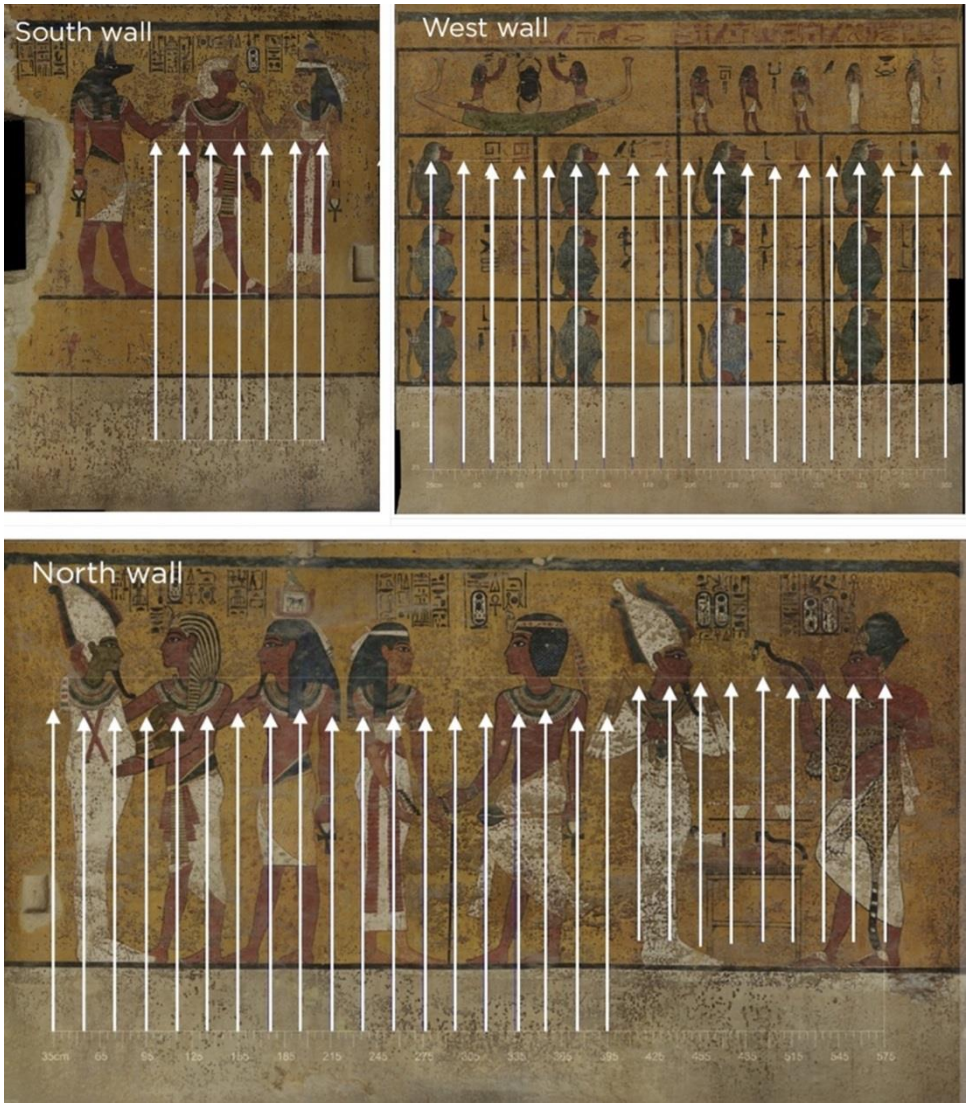

Figure 2S: *LF radar profiles acquired with the IDS TR200 GPR unit along the KV62 walls, the spacing among the lines is of 0.2 m.*

Note that in the NE corner of the North wall, the same wooden platform used for HF scans was adopted in order to pass over the sarcophagus lid, so that the starting acquisition height in this location was higher than for the other profiles.

The GPR profiles distribution for the IF dataset is shown in Figure 3S, where white arrows and the cyan arrows represent the respective distribution of the radargrams acquired in TM (336 radar profiles) and TE (126 radar profiles).

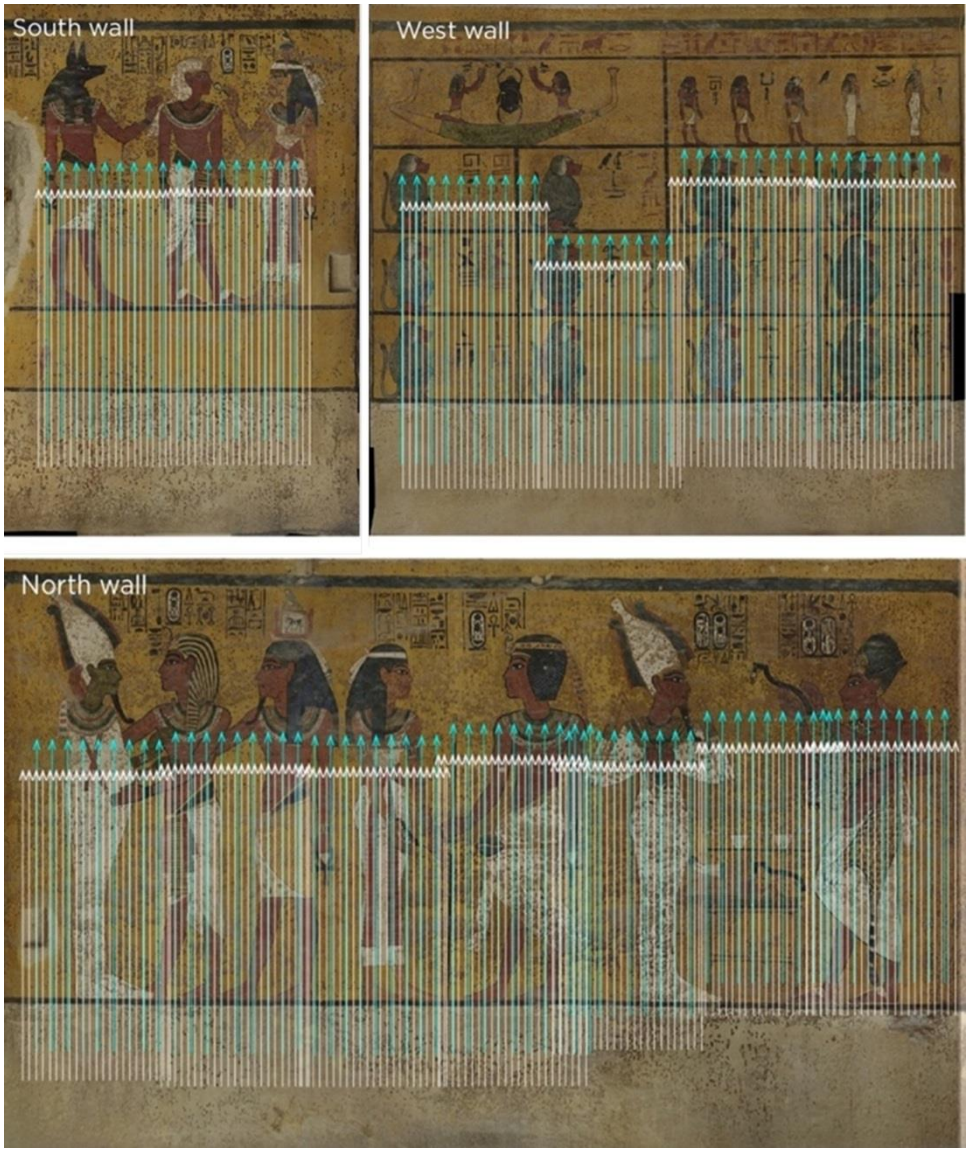

Figure 3S: *IF radar profiles acquired with the multi-channel IDS Stream-C system along the KV62 walls, white arrows represent the position of the radargrams acquired in TM-mode, at fixed spacing of 0.0435 m; cyan arrows represent radargrams acquired in TE-mode at fixed spacing of 0.099 m.*

2. Data processing

The three collaborating groups rocessed the data acquired with the different GPR systems independently and with different software, to avoid biasing and cross influences. Only after a satisfying processing step was reached we discussed and uniformed the processing flows in order to obtain a consistent result for all the surveys. Final processing steps adopted for the different GPR systems are hereafter reported.

2.1 High Frequency (HF) scans.

After many trials, a processing sequence that we consider appropriate in order to extract useful information without meaningful alteration of the raw data has been achieved for the HF scans. Data processing has been performed with Reflexw 8.55 (Sandmeier, 2018). The adopted processing steps were:

1. subtract-mean(dewow), to attenuate very low frequency components likely due to the acquisition setup;
2. move start time (-2.4 ns), to correct for the air gap between the antenna and the wall surface and to system delay;
3. divergence compensation, to recover the geometrical spreading of the wave front; since the e.m. properties of the plaster and of the hosting rock are not known with sufficient accuracy, we did not apply any other gain based on the physical attenuation;
4. bandpass 4-poles Butterworth filter (1400 – 3400 MHz), to attenuate low and high frequency noise in the traces; cut-off frequencies have been selected after spectral analysis carried out on randomly selected sample radargrams;
5. background removal, to remove strongly constant horizontal banding that, in this context, we attribute to a ringing of the pulse due to the air gap between the antenna and the wall and due to the widespread presence of the plaster;
6. spectral whitening, to widen the frequency band and shorten the pulse duration enhancing localized reflection events; this step is associated to a further bandpass four-poles frequency filter

(900-1200, 3700-4000 MHz) to further attenuate low and high frequency noise in the traces due to whitening;

7. time cut (36 ns), to focus the investigation onto a depth were we judge there is relevant information.
8. f-k velocity band-reject filter from 0.135 to 0.3 m/ns to further reduce any residual effects of the diffractions from the vertical lateral supports, still partially evident even after the wooden frame was adopted (see Sec. 2.1 above).

Examples of the results obtained by the adopted processing steps will be given in the following over calibration profiles. Finally, processed radargrams were assembled in space using the surveys reference system (see Figure 1 of the paper), while the software Voxler® 4.3.771 (Golden Software, Colorado, USA) was used to obtain a 3D imaging of the surveys. For this purpose, the absolute reflection amplitude was computed for each sample of the traces and the traces were interpolated with an inverse distance power-2 isotropic algorithm with a spatial resolution of 0.04 m in the x,y and z directions.

2.2 Low Frequency (LF) and Intermediate Frequency (IF) scans.

Raw data from LF and IF scans were post-processed and imaged with GPR-Slice software (Goodman et al, 1995; Goodman et al., 2004). The adopted processing steps were similar for the two surveys up to a certain level where dedicated processing was carried out. The processing steps for LF scans included:

1. move start time , to correct for the air gap between the antenna and the wall surface and for the system delay;
2. apply a gain function, to enhance the reflectors of interest without introducing clipping effects and artifacts into the data; a user defined gain function containing a linear component and an exponential compensation factor was applied. The total gain factor was selected according to the energy level exhibited by the radar pulse energy.
3. wobble noise correction; to attenuate the low frequency noise a wobble filter was used to compute a running average over a fixed scan length and then subtract it from the radar scans.

4. frequency-wavenumber (FK) filtering; after a spectral analysis was performed in the frequency-wavenumber domain, a FK filter was used to suppress the data noise observed by removing specific spatial frequency components.

5. bandpass filtering (128 - 365 MHz), to attenuate the horizontal band caused by the air gap between the antenna and the wall and to suppress high frequency noise.

6. Cepstrum deconvolution, to smooth out amplitude undulations in spectral frequencies, and to reduce the influence of multiple reflections.
7. Box-car filtering, to attenuate incoherent noise arising from the cepstrum deconvolution.

The same first three processing steps of LF scans have been used for IF scans also, followed by a bandpass filtering. Calibrated parameters have been adopted to account for the different radar system employed (i.e. for the IF scans the adopted parameters were: move start time of -12.8 ns and cutting frequencies of 330 and 890 MHz). A further spectral whitening step was also adopted, to equally weigh all the spectral components with the same magnitude and to increase the gain in portions of the radargrams with lower amplitude. The final processing step of IF data was a FK filtering similar to the one used for LF scans to attenuate the high frequency noise induced by the spectral equalization process.

Examples of the results obtainable with the adopted processing steps will be given in the following over calibration profiles. We finally Hilbert-transformed both LF and IF processed radargrams, in order to eliminate phase components before assembling the dataset and compiling 3D vector volumes. We also computed gain calibration curves for the multi-channel dataset to compensate variations in channels gain levels. Finally, we compiled GPR volumes using cell size of 0.05 m, where profiles spacing in the IF and LF ranges from 0.0435 to 0.2 m, and computed on a sequence of 269 and 225 height levels for the two respective datasets, corresponding to steps of about 0.01 m. We then interpolated the volumes along the cross-line direction only where gaps between adjacent lines exist. For this purpose, we compiled and interpolated two independent volumes for two walls oriented along the N-S and the E-W. We finally merged interpolated volumes into a unique 3D volume and smoothed with a 3x3x3 low pass filter.

3. Results over Calibration Profiles

Successful imaging of known voids and structures over calibration profiles was used to test the processing sequence and to evaluate the potentiality and limitations of the adopted surveying approach. In Figure 4S, examples of processed HF calibration profiles acquired along the East Wall of the Burial Chamber to the Treasury room (for the exact locations, see Figure 1 in the paper) are reported.

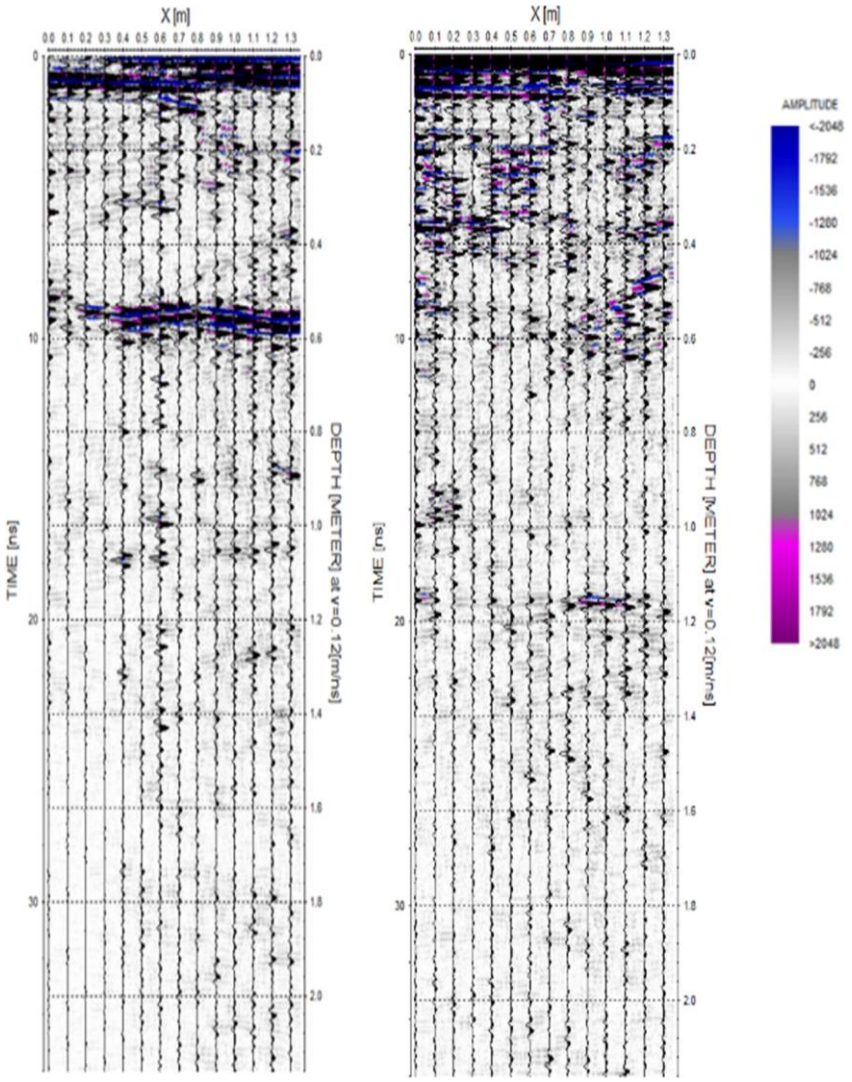

Figure 4S: *Processed HF calibration radargrams acquired from the Burial Chamber to the Treasury room (for exact location see Figure 1 in the paper): left) TE mode and right) TM mode.*

For these locations, the wall surface is cover by a plaster layer and by paintings similarly to the West and North walls of KV62 funerary chamber.

A clear difference can be observed in the two acquisition modes. The TE mode is successful in evidencing the presence of the void related to the Treasury room, with a clear reflection event located at a depth of 0.55 m, that matches the actual wall thickness in this particular location. Conversely, no clear reflections appear on the TM mode. The differences between the two acquisition modes go beyond those that are normally expected from the different polarizations over a reflecting plane parallel (even if gently “waving”) to the antenna profile. Similar differences and similar results have been also observed in the calibration profiles acquired from the Antechamber to the Annex (see Figure 1 in the paper), where only the TE mode was successful in locating the known void at a correct depth of 0.8 m. In this location the wall surface is free from the plaster.

Differences between the two acquisition modes are also observed in the HF calibration profiles acquired from the Treasury room to the Burial Chamber (also a plaster-free surface, for its exact location see Figure 1 in the paper) reported in Figure 5S.

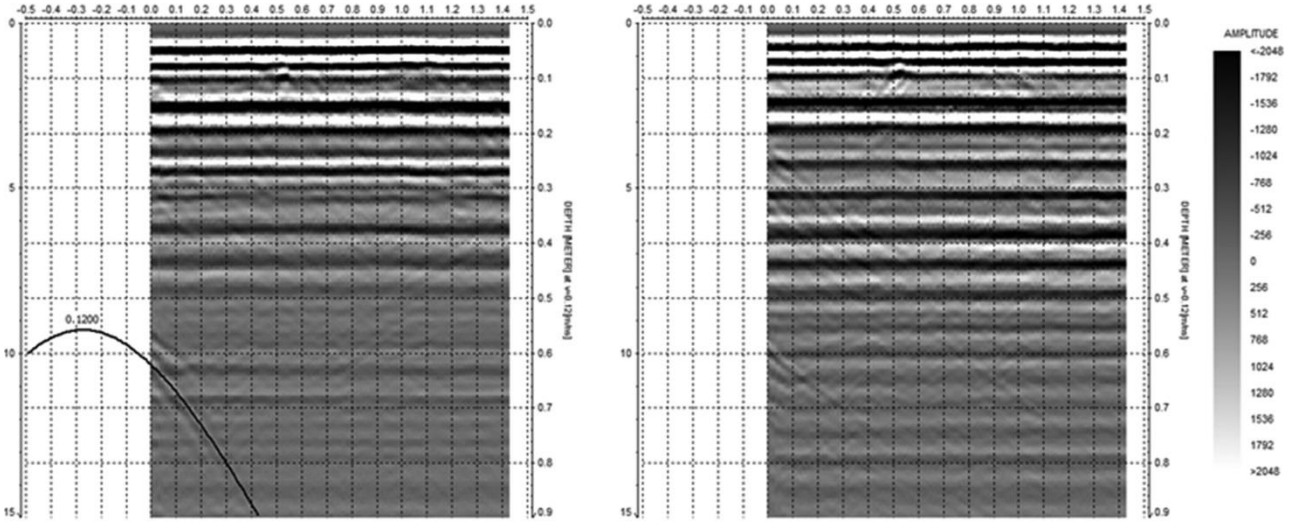

Figure 5S: *HF calibration radargrams, at processing step 02, acquired from the Treasury room to the Burial Chamber (for exact location see Figure 1 in the paper): left) TE mode and right) TM mode.*

A clear diffraction hyperbola is evidenced particularly for the TE mode. The hyperbola position, both in time and space, and the fact that it is much clearer in TE mode, led us to conclude that it is likely due to the corner of the door between the Burial chamber and the Treasury room. This has also been confirmed by forward modeling simulations of the radar wave propagation over an on-purpose built model of the Burial chamber. The aforesaid hyperbola gave also a clear estimation of the propagation velocity (0.12 m/ns) of the GPR pulse in the rock around the tomb.

We also performed calibrations profiles for LF and IF acquisition modes. The calibration profiles performed over known wall thickness ranging from 0.55 m (wall separating the Burial Chamber from the Treasury Room) to 0.8 m (wall between the Antechamber and the Annex) were successful in detecting the backwall and determining the correct thickness of the walls. In Figure 6S, examples of the calibration profiles for LF scans are reported, with similar results obtained also for the IF scans.

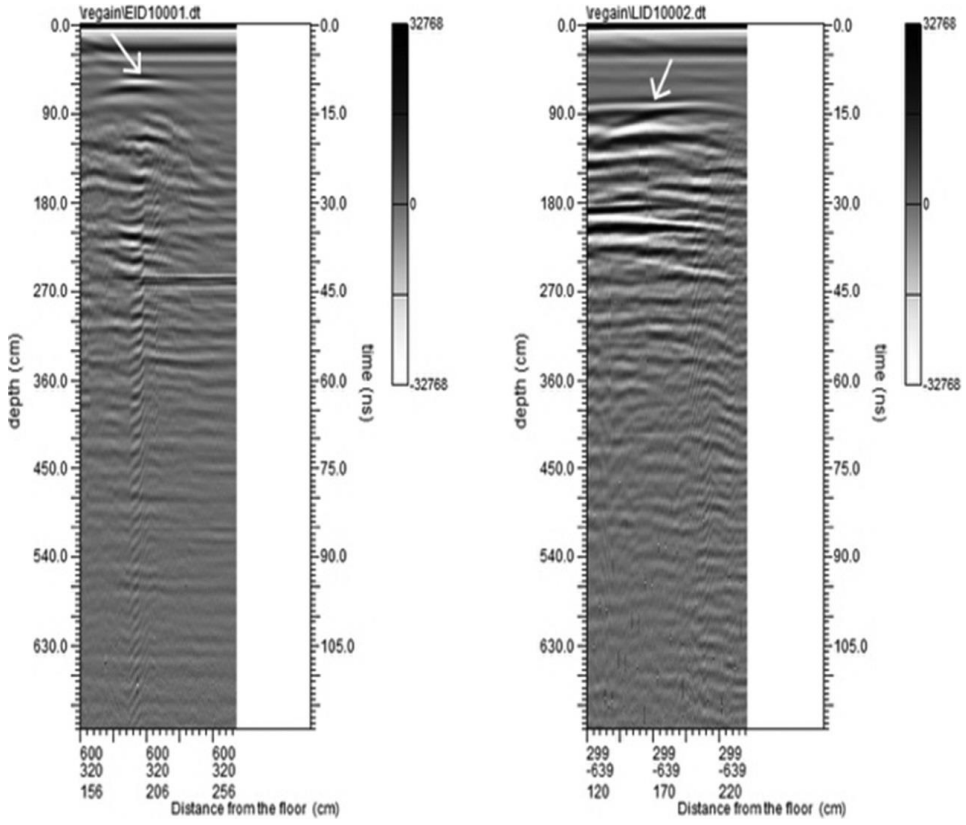

Figure 6S: *LF calibration radargrams, at processing step 03, acquired along the East Wall of the Burial Chamber toward the Treasury(left) and along the West Wall of the Antechamber toward the Annexe (right),for exact location see Figure 1 in the paper.*

Conversely, both IF and LF calibration profiles performed along the south wall of the Burial Chamber (for exact location see Figure 1) failed in locating the known void of the Annex at about 5 m depth. This gave us indications that attenuation factors are higher than expected and shorter maximum investigation depths, particularly for LF scans, should be expected.

In all the frequency bands used for our GPR scans, we found clear differences in the TE and TM modes of operation. In HF scans vertical corners (e.g. the corner of the door between the Burial chamber and the Treasury room in Figure 5S) are clearly, and correctly, detected in the TE mode acquisition and nearly absent in TM mode. On the other hand, we do not have a clear explanation for the very low reflection intensity of TM mode within the calibration profiles, where the reflectors are planes (even if gently "waving") parallel to the antenna profiles (the East wall of the Annex or the West wall of the Treasury). These differences go beyond those that that are normally expected from the different polarizations.